Tuning the Mechanical Properties of Graphene Oxide Paper and Its Associated Polymer Nanocomposites by Controlling Cooperative Intersheet Hydrogen Bonding

Owen C. Compton,[†,∥] Steven W. Cranford,[‡,∥] Karl W. Putz,[§] Zhi An,[†] L. Catherine Brinson,[§,*] Markus J. Buehler,[‡,*] and SonBinh T. Nguyen[†,*]

[†]Department of Chemistry, Northwestern University, 2145 Sheridan Road, Evanston, Illinois 60208, United States, [‡]Department of Civil and Environmental Engineering, Laboratory for Atomistic and Molecular Mechanics (LAMM), and Center for Materials Science and Engineering, Massachusetts Institute of Technology, 77 Massachusetts Avenue, Cambridge, Massachusetts 02139, United States, and [§]Departments of Mechanical Engineering and Materials Science and Engineering, Northwestern University, 2145 Sheridan Road, Evanston, Illinois 60208, United States. [∥]These authors contributed equally to this work.

ABSTRACT The mechanical properties of pristine graphene oxide paper and paper-like films of polyvinyl alcohol (PVA)-graphene oxide nanocomposite are investigated in a joint experimental–theoretical and computational study. In combination, these studies reveal a delicate relationship between the stiffness of these papers and the water content in their lamellar structures. ReaxFF-based molecular dynamics (MD) simulations elucidate the role of water molecules in modifying the mechanical properties of both pristine and nanocomposite graphene oxide papers, as bridge-forming water molecules between adjacent layers in the paper structure enhance stress transfer by means of a cooperative hydrogen-bonding network. For graphene oxide paper at an optimal concentration of ~5 wt % water, the degree of cooperative hydrogen bonding within the network comprising adjacent nanosheets and water molecules was found to optimally enhance the modulus of the paper without saturating the gallery space. Introducing PVA chains into the gallery space further enhances the cooperativity of this hydrogen-bonding network, in a manner similar to that found in natural biomaterials, resulting in increased stiffness of the composite. No optimal water concentration could be found for the PVA-graphene oxide nanocomposite papers, as dehydration of these structures continually enhances stiffness until a final water content of ~7 wt % (additional water cannot be removed from the system even after 12 h of annealing).

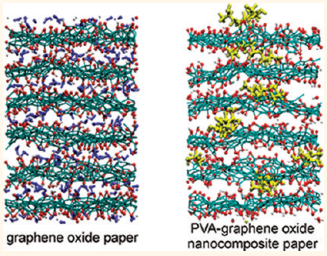

KEYWORDS: graphene oxide · graphene oxide paper · polymer nanocomposite · mechanical properties · molecular dynamics simulations

Graphene oxide, an oxygenated derivative of graphene, has been employed in the fabrication of myriad materials[1] with a wide variety of applications including supercapacitors[2] and drug delivery vehicles.[3] This broad application range is made possible given the versatile chemical composition of these two-dimensional nanosheets, which feature hydroxyl and epoxy groups on the basal plane along with carboxyl and carbonyl moieties lining the nanosheet edge.[4,5] Among the many macroscopic structures that have been made from graphene oxide, one of the most remarkable is graphene oxide paper, a self-supporting thin film consisting of aligned graphene oxide nanosheets.[8] These ordered structures exhibit excellent mechanical properties (stiffness up to 40 GPa, in the range of engineered materials such as concrete,[6] and tensile strength up to 125 MPa, similar to that of cast iron[7]) while remaining highly flexible and ductile.[8] This desirable combination of properties has been attributed to the numerous hydrogen-bonding interactions between adjacent layers in the paper structure, as mediated by a small number of intercalated water molecules (~5–15 wt %) that interact with the functional groups on the adjacent nanosheets (Figure 1a).[9,10] The ensuing multitude of water–water, water–nanosheet, and nanosheet–nanosheet hydrogen bonds have been proposed to generate a hydrogen-bonding network that strengthens the paper structure dramatically. Indeed, when water (both a hydrogen-bond acceptor and donor) is intercalated within graphene oxide paper, its stiffness and strength are respectively 35% and 25% greater than when *N*,*N*-dimethylformamide (DMF, a hydrogen-bond acceptor only) is present in the intersheet gallery.[10]

Hydrogen-bonding networks, similar to that proposed in graphene oxide paper, are known to play an important role in enhancing the mechanical properties of several natural materials.[11] For example, spider silk features a robust network of

* Address correspondence to cbrinson@northwestern.edu (for mechanical studies), mbuehler@MIT.EDU (for theoretical work), stn@northwestern.edu (for materials synthesis and fabrication).

Received for review August 2, 2011 and accepted December 21, 2011.

Published online December 21, 2011
10.1021/nn202928w

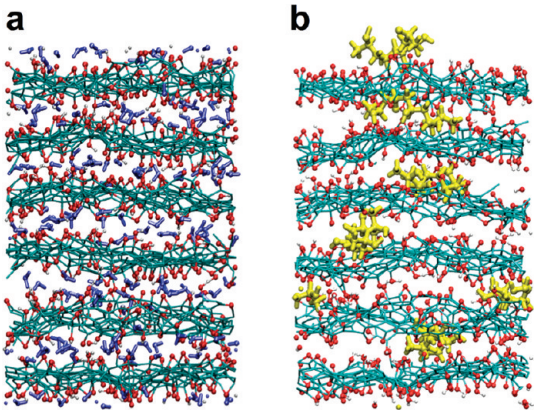

Figure 1. Model snapshots of (a) a stack of pristine graphene oxide nanosheets with intercalated H_2O (10% water content shown) and (b) a PVA-GO composite (5.5 wt % polymer content shown). These lamellar models were subjected to equilibration, with the equilibrium spacing (s_{eq}) determined by averaging the five gallery spacings.

hydrogen bonds between aligned β-sheet crystals that is key to its exceptional tensile strength and extensibility.[12,13] Likewise, a hydrogen-bonding network plays a vital role in maintaining the strength and elasticity of the triple helix in collagen.[14,15] Unfortunately, water molecules are limited to confined *molecular-scale* regions within the aforementioned biomaterials,[13,16] making it difficult to systematically analyze dehydrated forms of these structures. In contrast, water content in the graphene oxide paper structure can be readily tuned in a similar fashion to the hydration of lamellar clays,[17,18] given the large repeat distance of adjacent graphene oxide nanosheets (~6–11 Å)[8,19,20] that can accommodate a wide variety of water compositions. To our advantage, graphene oxide paper also has significant long-range order, allowing the water intercalation process to be readily monitored by powder X-ray diffraction[21] (PXRD) in the same fashion as the swelling of clay.[22]

The strong influence of intercalated water on the structure of graphene oxide paper[8,9,23] or its unexfoliated precursor, graphite oxide (GO),[20,24,25] has been reported in the literature, with multiple studies revealing tunable properties through variation of water content. For example, increasing the water content in the interlayer spacing of graphene oxide paper has been known to cause swelling,[23] with decreasing mechanical stiffness,[8] in a similar fashion to cellulose-based paper.[19] Previous studies have suggested that such changes in the mechanical properties of graphene oxide paper are linked to the presence of water molecules in its intersheet gallery space,[8,9] which greatly change its mechanical properties through hydrogen bonding to the multitude of functional groups on adjacent sheets in the paper structure. As this hypothesis was not systematically explored, either experimentally[8] or theoretically,[9] we were prompted to quantify the contribution of intercalated water to the mechanical properties of graphene oxide paper as well as the role that polyvinyl alcohol (PVA, a material that not only is water-like in its hydrogen-bonding ability, but also possesses strong covalent bonds between the hydrogen-bonding-capable repeating units) plays in a PVA-graphene oxide nanocomposite film. We further hypothesize that the macroscopic mechanical properties of these paper-like materials can be tuned through the precise control of their molecular composition (i.e., the water molecules and polymer chains in the gallery space of these graphene oxide based material), unlike the aforementioned natural protein-based materials, whose compositions are not readily modifiable.[26]

Herein, we report a combined experimental–theoretical study that elucidates the crucial role played by intercalated water molecules in stiffening the lamellar structure of graphene oxide paper, where an optimal amount of water affords maximum stiffness. Very small changes (~1 wt %) above and below this optimal water content lead to *dramatic* decreases in the storage modulus, or stiffness, of the structure in a manner that was previously unobserved.[8,9] Extending this concept further, an associated PVA-graphene oxide nanocomposite (Figure 1b) was also investigated to vary the hydrogen-bonding capacity of the interlayer gallery and explore the effect of incorporating covalent bonding into the gallery spacing of graphene oxide paper, much like the multicomponent structures found in natural biocomposites. As expected, the effect of water content on the stiffness of the paper is reduced when PVA is present; continual dehydration of the structure serves only to increase the storage modulus of the composite. Full atomistic reactive molecular dynamics (MD) simulations reveal the discrete nature of the hydrogen-bonding networks in both pristine graphene oxide and PVA-graphene oxide papers to elucidate the mechanisms involved in their stiffening of these structures as they cross-link adjacent sheets in a stack of graphene oxide nanosheets. These modeling results were then used to interpret the mechanisms that govern the macroscopic material properties of graphene oxide paper and its associated composites.

RESULTS AND DISCUSSION

Mechanical Properties of Pristine Graphene Oxide Paper. To quantify the relationship between the interlayer water content and the mechanical properties of graphene oxide paper, we monitored the dynamic variance in the storage modulus of as-prepared graphene oxide paper during a controlled dehydration. Several thin strips of graphene oxide paper were heated at 95 °C in the oven of a dynamic mechanical analyzer (DMA), with only one strip mounted on the sample stage for continuous modulus measurements. Over the course of the DMA experiment, as water was slowly evaporated from the strips, the unmounted samples were removed and

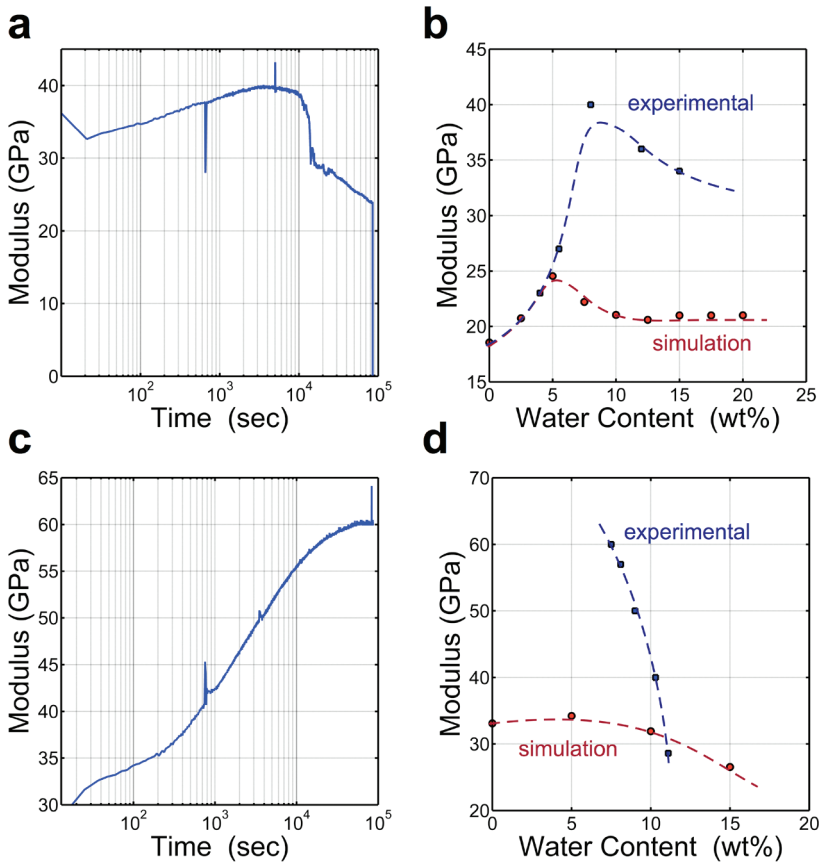

Figure 2. (a) Time-resolved plot of the dynamic storage modulus of a sample of graphene oxide paper during dehydration at 115 °C. (b) Experimental and simulation plots of the storage modulus of graphene oxide paper as a function of water content. (c) Time-resolved plot of the dynamic storage modulus of a PVA-graphene oxide nanocomposite paper during dehydration at 115 °C. (d) Experimental and simulation plots of the storage modulus of PVA-graphene oxide composite paper as a function of water content. The experimental composite contains 22 wt % PVA whereas simulated model contains 5.5 wt % PVA. All dashed lines are included only as guides to the eye.

subjected to coulometric Karl Fischer water titration. At the beginning of the experiment, the graphene oxide paper was found to have a storage modulus of 34 GPa with a corresponding water content of ~15 wt %, a value commonly observed in unexfoliated GO powder.[25] As the samples were continually dehydrated in the DMA oven, its modulus increased to 40 GPa at a water content of ~7 wt %. Further dehydration to the lowest achievable water content (~4 wt %) dramatically decreases stiffness to only 23 GPa, suggesting the presence of an optimal water content at which the paper structure achieves maximum stiffness (Figure 2b). Assuming continual dehydration during the course of our experiment, this enhancement and degradation of storage modulus is most striking when viewed as a function of time (Figure 2a). The dramatic enhancement of modulus after ~4000 s of annealing at 95 °C,[27] followed by a quick decline in stiffness, illustrates the crucial role that water molecules play in affecting the mechanical properties of graphene oxide paper.

To simulate the aforementioned experimental system, graphene oxide paper models were constructed from four and six layers of nanosheets, with periodic boundaries as depicted in Figure 3. We note that the relatively homogeneous bulk structure of graphene oxide paper makes it an ideal candidate for a parametric study, wherein the regular stacked geometry facilitates the construction of a representative, fully atomistic, model system. We intentionally limited nanosheet−nanosheet interactions (i.e., those that occur directly between two layers when they come in contact) by imposing idealized geometries and boundary conditions so that the effect of hydrogen bond density in the interlayer spacing can be isolated. Thus, the interactions between layers of graphene oxide consist of weak dispersive attractions (van der Waals), Coulombic forces, and hydrogen bonding between the epoxy and hydroxyl groups on the basal plane.[19,28,29] The surface energy of two simulated graphite oxide sheets with a stoichiometry of $C_6O_3H_1$ in a vacuum was determined by MD energy minimization to be ~516 mJ m^{-2}, in the vicinity of the adhesion energies of pristine graphene (from 260 to 345 mJ m^{-2}), previously determined by computational and experimental investigations.[30−32] For comparison, this value is an order of magnitude higher than the adhesion energies (48.6 to 62.5 mJ m^{-2}) reported for the spatulae of a

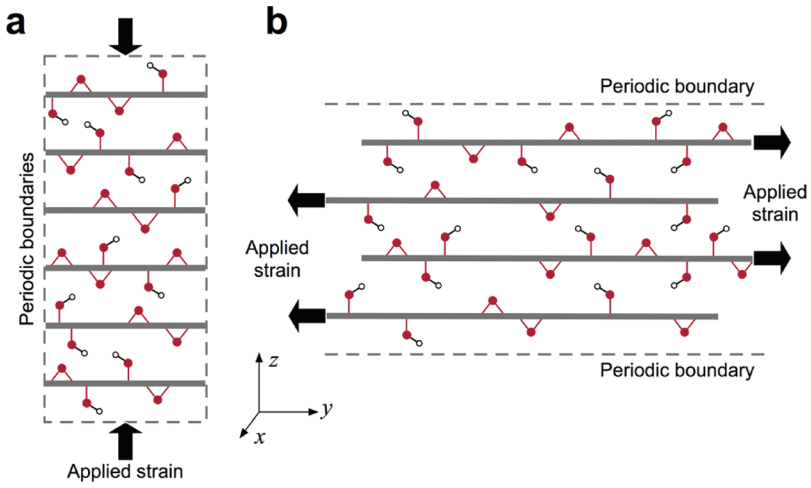

Figure 3. (a) Multilayer axial or "*stacked*" model of graphene oxide paper consisting of six 25 Å × 25 Å sheets with periodic boundary conditions implemented along sheet edges to represent continuous graphite oxide in-plane and continuity along the strain axis. The initial interlayer spacing is set larger than the unknown equilibrium spacing (s_{eq}) to allow placement of water and PVA molecules. (b) Multilayer shear or "*transverse*" model consisting of four 50 Å × 100 Å sheets staggered by 10 Å in the longitudinal direction; periodic boundary conditions implemented along the short direction (*x*-axis) and out-of-plane direction (*z*-axis) to allow shear loading of the system without direct stretching of the graphene oxide nanosheets. Shear-strain loading was applied to measure the stiffness of the hydrogen-bonded structure in the shear direction.

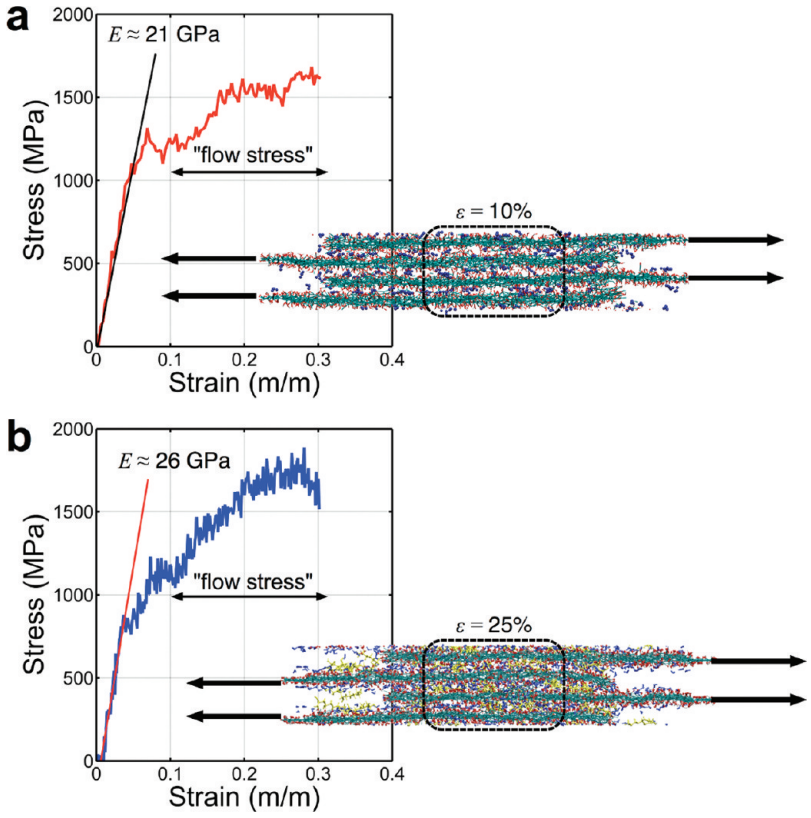

Figure 4. (a) Simulated stress–strain curve for a graphene oxide paper containing 2.5 wt % water. Stiffness (modulus) is fitted to the initial, linear regime of the stress–strain profile (~21 GPa). The inset model snapshot was captured at 10% strain, where virial stress was calculated on the interior region (encircled in the inset) of the structure. (b) Simulated stress–strain curve for a PVA-graphene oxide nanocomposite paper containing 5.5 wt % PVA and 15 wt % water. Stiffness (modulus) is fitted to the initial, linear regime of the stress–strain profile (~26 GPa). The inset model snapshot was captured at 25% strain, where virial stress was calculated on the interior region (encircled in the inset) of the structure.

gecko,[33] noted for its dry-adhesion capabilities. We note, however, that such high surface energy in the paper structure is only applicable in a vacuum and physically unattainable in solution, as epoxy and hydroxyl functional groups imbue the nanosheets with a strongly hydrophilic character. It is this hydrophilicity that allows

graphite oxide and graphene oxide paper to readily swell in water to variable interlayer distances ranging from approximately 6 to 11 Å,[8,19,20] depending upon the water content of the experimental sample.

The experimental DMA measurements were then simulated by *in silico* pulling of the alternating layers in a four-layer model in opposite directions, resulting in stress−strain curves from which stiffness (modulus)[34] can be extracted (Figure 4). These simulated values nicely confirm the presence of our experimentally determined optimal water content. The simulated modulus was found to remain at a constant ~21 GPa value when the water content was kept in the high (10−20 wt %) range (Figure 2b). As the water content was lowered to 5 wt %, a maximum modulus of ~25 GPa was observed. This optimal point is similar to that observed in our experiment, further supporting the hypothesis that intercalated water is a key contributor to the mechanical properties of graphene oxide paper (Figure 2b). As in the experimental study, stiffness was found to decrease when the water content was lowered past the optimal 5 wt % value. Notably, a completely dehydrated structure, which cannot be achieved in experiment, resulted in a modulus of 18 GPa, significantly below that of water-intercalated samples.

As shown above, the modulus values obtained from our molecular simulations are substantially lower than the experimentally measured stiffness of the paper. Such variance can be attributed to the ideally applied *in silico* loading, where alternating graphene oxide sheets are strained perfectly in-plane during molecular simulations, eliminating any potential for sheet misalignment, entanglement, or edge effects. Our idealized graphene oxide paper model consists of stacked graphene oxide sheets of infinite extent (Figure 1a), while the actual material comprises randomly stacked nano- and micrometer-sized nanosheets that are likely crumpled, folded, and entangled with each other. Consequently, the load-transfer mechanism among the neighboring graphene oxide sheets in the experimental sample would include strengthening mechanical interactions that significantly deviate from the simple computational model. Additionally, the stress extracted from the MD simulations is solely the uniaxial component of the virial stress [see Supporting Information (SI)], where the load is only transferred through the interlayer hydrogen-bonding network that bridges adjacent sheets. In this way, any possible contribution from the shear effects that are likely present during experimental measurements would be neglected and a lower stiffness compared to experimental data is expected. We note that a previous full atomistic study of graphene oxide paper, where stiffness was calculated using atomistic displacement correlation functions normal to the graphene oxide basal plane, reported stiffness values that are in the same range as our work.[9]

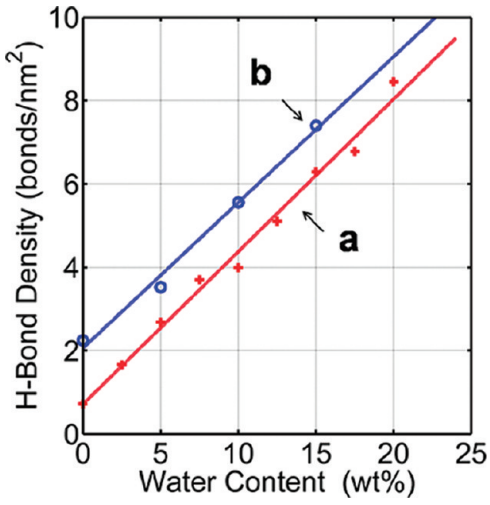

Figure 5. Plots of hydrogen-bonding density for (a) graphene oxide paper and (b) PVA-graphene oxide nanocomposite paper as a function of water content. The lines are linear fits to the data.

In silico compression of the six-layer stack further confirmed the competency of our simulated model by capturing a proportional relation between the intercalation-induced increases in interlayer distance and water content, from approximately 5.5 to 6.6 Å over the 0−20 wt % range of water content (Figure S1 in the SI). While these values are lower than those previously reported for graphene oxide paper (~8−10 Å),[8] the relatively small scale of our molecular model, combined with periodic boundary conditions, limits out-of-plane rippling of individual graphene oxide layers and is representative of a relatively flattened ideal stacking. In addition, it is expected that smaller interlayer spacings would result from the MD simulations due to the relatively small, periodic, planar arrangement that precludes mismatched edges and misaligned layers. We note that our simulations were carried out with a homogeneous distribution of water in each interlayer gallery to limit the potential for the clustering of water molecules observed in previous MD simulations,[9] reduce any discontinuities in the behavior of the layers, and match the narrow distribution of intersheet spacings observed experimentally in PXRD.

Mechanisms for Stiffness Variance in Pristine Graphene Oxide Paper. Under the ideally applied strain conditions of our MD simulations, water molecules only contribute to the stiffness of the graphene oxide paper structure *via* the hydrogen bonds that they form between adjacent layers. Given the finite number of oxygen-containing functional groups on the graphene oxide surface, there is an upper bound to the number of potential locations where water molecules can form hydrogen-bonding intersheet bridges. Once this limit is reached (Figure 2b), additional intercalation of water molecules into the intergallery spacing simply serves to swell the structure and facilitate lateral "sliding" of

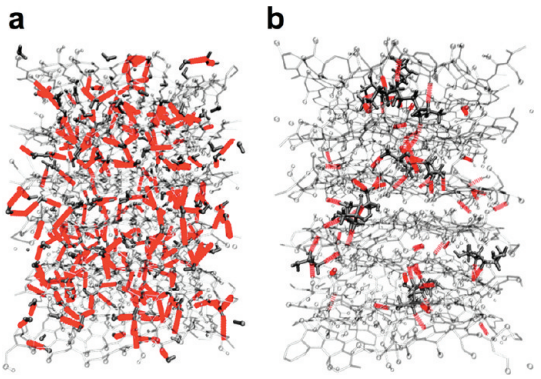

Figure 6. Model snapshots highlighting the hydrogen-bonding networks between the graphene oxide nanosheets in (a) a graphene oxide paper and (b) an ~5.5 wt % PVA-graphene oxide nanocomposite paper. While water molecules are included in the simulations for both models, water molecules were not shown in the snapshot of the composite model to emphasize the clusters of hydrogen bonds that form between PVA and the nanosheets in this system.

the nanosheets. Thus, an optimal water content exists that maximizes the mechanical properties of the structure and minimizes this extraneous "sliding". *In silico* equilibration of hydrogen bond density in the paper structure over a range of water content reveals an almost-linear relation between this variable and the number of water molecules (Figure 5). Approximately 9 ± 0.4 hydrogen bonds/nm^2 exist at 20 wt % water content, a slightly lower value than previously observed in studies with more reduced graphene oxide models[9] (~10 and 15 hydrogen bond/nm^2 for $C_{10}O_2(OH)$ and $C_{10}O_2(OH)_2$ stoichiometries, respectively). The higher concentration of epoxy and hydroxyl groups in our model, which more accurately reflect the compositions in our experimental samples (see elemental analysis data in the SI), serve to limit hydrogen bonding between water molecules and yield a more homogeneous (i.e., no clustering) distribution of hydrogen bonds in the gallery space (Figure 6). Such homogeneity is key to the consistent estimates of paper stiffness in our MD simulations.

The balance of hydrogen-bond acceptors and donors between intercalated water and graphene oxide layers plays a crucial role in determining the optimal water content for the graphene oxide paper structure, at which point the modulus peaks. Based on the $C_6O_2(OH)$ stoichiometry, the nanosheets in our molecular model were found to exhibit a maximum modulus when a sufficient number of water molecules (~100 water molecules per interlayer spacing, or 2 molecules/nm^2 at 5 wt % water content) are present to maximize the amount of interlayer bridges to ~70 hydroxyl groups and ~35 epoxy groups per layer, leaving no underutilized functional groups on the nanosheet surface. Given the random distribution of hydroxyl and epoxy groups on graphene oxide, the addition of more water molecules optimizes the necessary interlayer bridging with efficient molecular packing, where extraneous water molecules are homogeneously distributed throughout the intersheet gallery, forming multiple water–water interactions in addition to water–nanosheet hydrogen bonds. At 10 wt % water content (~200 water molecules per interlayer spacing, or 4 molecules/nm^2), the amount of water in the gallery spacing far exceeds the available hydroxyl and epoxy groups, saturating the interlayer gallery with superfluous water molecules. While the total number of hydrogen bonds increases due to water–water hydrogen bonding, there is no increase in the stiffness of the graphene oxide paper, as the interlayer network is weakened by the addition of numerous water–water interactions. These additional degrees of freedom allotted to the hydrogen-bonding network then allow for the reorientation of water molecules with minimal strain,[10] thus overwhelming the stiffness-inducing water–nanosheet interactions.

Upon the introduction of tension, the stress–strain response of our *in silico* model (Figure 4) initially exhibits an approximately linear regime from which the modulus can be calculated. A yielding occurs in the range of 3–4% strain, followed by a regime of almost constant, or "flow", stress. For example, at 15 wt % water content, the flow stress is on the order of 1100–1800 MPa and can be attributed to the plastic deformation of the paper caused by the breaking and reformation of the hydrogen bonding network as the graphene oxide layers slide past each other. Unfortunately, as flow stress is determined on a nanosecond time scale, well below the resolution of our dynamic mechanical analyzer, its behavior cannot be accessed experimentally. The reformation of hydrogen bonds in this system prompted an analysis of their evolution under strain (Figure 7). As the layers are equilibrated during MD simulation, water–water, water–nanosheet, and nanosheet–nanosheet hydrogen bonds form to generate interlayer bridges. Under strain, we observe a maximum hydrogen-bond content during the initial elastic response where the stiffness was calculated. The onset of yield corresponds to a drop in the number of hydrogen bonds, whose magnitude is independent of the variation of water content, indicating the failure of multiple hydrogen bonds simultaneously upon yield. The number of hydrogen bonds then remains approximately constant under further strain, with this region encompassing both water–water and intralayer (i.e., where the water molecule forms more than one hydrogen bond with the same nanosheet) hydrogen bonds. While these nonbridging hydrogen bonds are merely carried along during deformation and do not contribute to the overall mechanical stiffness or stress of the paper structure, they are not held at a constant configuration but are subjected to breaking and reformation as water

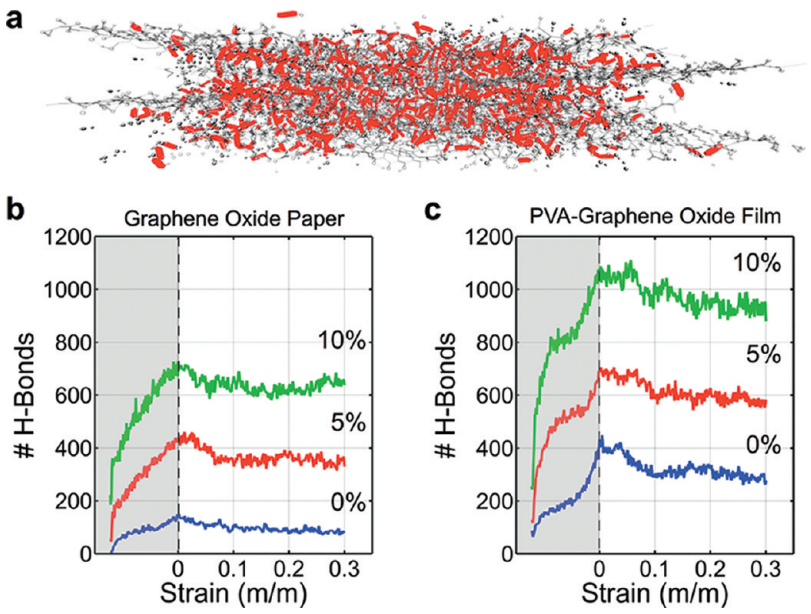

Figure 7. (a) Model snapshot highlighting the dense hydrogen-bonding network in a PVA-graphene oxide nanocomposite structure containing 5.5 wt % PVA and 15 wt % water. (b and c) Plots depicting the total number of hydrogen bonds as a function of applied strain for graphene oxide paper (b) and a 5.5 wt % PVA-graphene oxide nanocomposite (c) at water contents of 0, 5, and 10 wt %. Shaded regions indicate that the system was subject to energy minimization and equilibration, not applied strain.

molecules reconfigure, resulting in a "flow-stress" regime.

Our combined experimental and simulation data reveal two main reasons for the existence of an optimal water concentration in the graphene oxide paper structure. First, water is necessary in the structure to bridge the hydrogen-bonding sites (i.e., the hydroxyl and epoxy) on the adjacent nanosheet surface. The generated hydrogen-bonding network produces robust interlayer connections, while marginally affecting interlayer spacing; however, introducing additional water in the structure causes superfluous water−water hydrogen bonding (clustering/aggregation) and induces swelling that weakens the interlayer bridges. Second, the reversible nature of the hydrogen bonds allows for the breaking and reformation of those bonds under strain,[12] with optimal water content ensuring the reformation of interlayer bridges, rather than passive water−water clusters or direct intrasheet connections.

As discussed above, our results mark the first time that the mechanical properties of graphene oxide paper were observed, by both experiment and modeling, to vary significantly in such a small range of water content (5−8 wt %). Our results quantify a relationship previously reported in experiments that only qualitatively observed increased stiffness during the dehydration of graphene oxide paper.[8] In addition, it fills in the gap left by a theoretical manuscript[9] that discusses only initial values of graphene oxide paper stiffness, as determined by atomic displacement correlation functions, leaving unaccounted any changes in the hydrogen bond network during tension. We note that the water-content increments (∼1, ∼10, ∼15, and ∼25 wt % water) studied in this reference was probably too coarse to catch the small optimal water content that we found herein, especially as the hydrogen-bonding network was changed during tension.

Mechanical Properties of PVA-Graphene Oxide Nanocomposite Paper. From the discussion above, water molecules clearly play a key role in affecting the stiffness of pristine graphene oxide paper, which have only two components (stiff nanosheets and water molecules). While this simple system can be easily evaluated by our model, many natural materials, like nacre, contain a flexible protein (chitin and lustrin) component in addition to a stiff inorganic (aragonite platelets) material and molecular water.[35] To better mimic these more complex materials (and to probe the effect of controlling the organization of H-bonds at the molecular level), we incorporated a moderate amount (22 wt %) of PVA into the graphene oxide paper structure to serve as the flexible component that can interact strongly with the stiff graphene oxide nanosheets. Such composite papers can be readily fabricated *via* vacuum-assisted self-assembly (VASA),[10] where the dissolved polymer is combined with the graphene oxide dispersion prior to the generation of the desired layered paper structure featuring intercalated polymer chains between the graphene nanosheets. Not surprisingly, the presence of PVA within the paper structure significantly modifies its behavior during dehydration. Low-temperature annealing (115 °C) of the PVA-graphene oxide composite paper consistently enhances the storage modulus from an original value of 35 GPa at

12 wt % water up to 55 GPa at 7 wt % water after 24 h of treatment (Figure 2a and 2c). This increase in modulus, which occurs as the nanocomposite is dehydrated, further emphasizes that PVA can effectively replace water in forming the hydrogen-bond network that serves to stiffen the paper structure. Since no further dehydration could be achieved in the composite sample, even after 95 h of annealing under our experimental conditions, this is likely the minimum amount of water achievable in the sample at atmospheric pressure. That this minimum water content is greater than the amount observed for pristine graphene oxide paper suggests that some water molecules may be trapped within the PVA chains in the interlayer gallery, not surprisingly given the known hygroscopic nature of PVA.[36] While this "trapping" of water may preclude the conclusive determination of whether an optimal water content exists in our PVA-graphene oxide composite, our theoretical work suggests its absence in the composite system (see next paragraph).

MD simulations using a six-layer PVA-graphene oxide stack (Figure 1b) confirm the experimental DMA results for this composite system, where the removal of water molecules from the structure continually enhances stiffness. We note that our MD simulations utilized a model containing a smaller amount of PVA (5.5 wt %) than our experimental paper sample (22 wt %) due primarily to modeling constraints. During model construction, the algorithm used for the random addition of PVA chains into the paper structure becomes hindered at PVA contents exceeding ~10 wt %, as the water molecules do not sufficiently disperse among the polymer chains during the short equilibration period (restricted by computational cost). Under such nonequilibrium conditions, planar arrangement of nanosheets is lost under tension, and the effect of varying water concentration is more difficult to quantify. Fortunately, since interactions between PVA, nanosheet, and water occur exclusively through hydrogen bonding, the behavior of composites with different compositions should qualitatively agree, as in the case of our experimental (22 wt % PVA) and simulated (5.5 wt % PVA) systems. We note that our simulations of the composite with 5.5 wt % PVA show a homogeneous distribution of the polymer chains that exclude the possibility of having gallery regions that are void of the effects from PVA chains.

Interestingly, the addition of PVA into the structure increased the interlayer spacing more drastically than the addition of water (see Figure S1 in SI), as the larger PVA oligomers cannot disperse throughout the interlayer spacing as efficiently as the smaller water molecules. This results in several "cavities" between PVA and the nanosheet surface, where many of the sheet-bound hydroxyl and epoxy groups do not form hydrogen bonds with the PVA but with water molecules. In this sense, water molecules can readily serve to bridge PVA and graphene oxide, utilizing all sheet-bound functional groups. Such cavities afford a more heterogeneous distribution of interlayer bridges, where the pendant hydroxyl groups of PVA form clusters of hydrogen bonds with the nanosheet surfaces (Figure 6b). Due to the presence of the polymer backbone, these hydrogen-bonded clusters form a more-stable arrangement than the homogeneous distribution of hydrogen bonds in the graphene oxide paper (Figure 6a), providing a shared cooperative mode of stress transfer by means of the polymer backbone. Previous studies concerning hydrogen-bond assemblies in proteins (β-strands and β-sheet structures) have suggested that hydrogen bonds deform cooperatively within small protein domains to achieve maximum strength, with clusters limited in size to only a few hydrogen bonds.[13,37,38] Similar cooperativity is exploited in our model by the limited number of epoxy and hydroxyl groups in the vicinity of each PVA chain.

While further stiffening of the PVA-graphene oxide structure at lower water concentrations may be expected (as in the pristine graphene oxide sample), when the water content in our composite model (5.5 wt % PVA) was varied from 0 to 20 wt %, little variation in stiffness was observed from 0 to 5 wt % (33 to 34 GPa). Past a 5 wt % water-content "saturation point", the addition of water into the system constantly degraded stiffness with the modulus falling to 27 GPa at 20 wt % water (Figure 2c), suggesting that excess water molecules in the composite structure promoted water−water, water−PVA, and water−nanosheet interactions that then replaced the original structure-stiffening direct PVA−nanosheet hydrogen bonds with these weaker links or bridges. In this sense, too much water would be detrimental to the composite structure, since there is less likelihood for direct transfer of stress between the mechanically robust components of the composite. Notably, the stiffness of the theoretical PVA-graphene oxide composite is again lower than that observed experimentally at all water concentrations (Figure 2d). Along with the previous differences between our experimental and theoretical results discussed (e.g., ideal loading and system geometry), this discrepancy can further be attributed to both the difference in polymer chain length (~50 repeat units in experiment vs 5 repeat units in simulation) and content (22 wt % in experiment, 5.5 wt % in simulation) between our two evaluation methodologies.

Mechanisms for Stiffness Variance in PVA-Graphene Oxide Nanocomposite Paper. In agreement with a previous investigation,[9] we found that the graphene oxide layers in the PVA-graphene oxide paper structure are interlinked *via* a *nonuniform* network of hydrogen bonds mediated by oxygen-containing functional groups, water molecules, and PVA chains. PVA was found to replace some of the water molecules in

intersheet hydrogen bonding and enhance the structure stiffness in comparison to the pristine graphene oxide paper at the same water content. Interestingly, the addition of PVA to graphene oxide paper appears to result in a much higher capacity of the structure for hydrogen bonding, up to a 50% increase for equivalent levels of hydration. Similar to that observed in the pristine graphene oxide, the PVA-graphene oxide composite model exhibits a maximum hydrogen-bond content during the initial elastic response. Analysis of the stress–strain response of a 5.5 wt % PVA-graphene oxide composite structure reveals a linear response until rupture of the hydrogen-bonding network, followed by yielding from ~4 to ~6% strain (Figure 4, for representative stress–strain responses; Figure 7 for the decrease in the number of hydrogen bonds). This yield strain is marginally greater than that of the pristine graphene oxide system and can be attributed to the initial alignment of PVA chains to the direction of strain prior to hydrogen-bond-based stress transfer upon the introduction of tension. As in the pristine graphene oxide structure, the system is again subjected to "flow stress" after yielding, which correlates to the plastic breaking and reformation of the hydrogen-bonding network. This heterogeneous network facilitates a smooth failure at the molecular scale, allowing for the formation of secondary PVA-nanosheet hydrogen bonds during deformation. Notably, the forced cooperativity of hydrogen bonds in the composite system, where the polymer backbone naturally groups the bonds into finite clusters, also serves to enhance stiffness in this structure. Together, the resulting nonuniform distribution of hydrogen bonds between PVA and nanosheet increases the cooperativity of those weak bonds to maximize stiffness, as they can cumulatively transfer more stress than water molecules alone.

CONCLUSION

In summary, we have demonstrated the key role that water molecules play in affecting the mechanical properties of pristine graphene oxide paper and its associated polymer nanocomposites. As in a number of natural materials, water molecules assemble into a hydrogen-bonding network that is crucial to the observed stiffness of these paper-like materials. For single-component graphene oxide paper, a maximum experimental stiffness of 40 GPa is achieved at an optimal water content of ~7 wt %, above and below which point stiffness is significantly lowered. Theoretical simulations of the graphene oxide paper structure reveal a similar optimal water content where the presence of the peak modulus can be attributed to the saturation of water-mediated interlayer hydrogen bonds. While addition of more water beyond this optimal water content increases the density of hydrogen bonds in the gallery space, the network becomes dominated by water–water hydrogen bonds that do not bridge adjacent nanosheets and only serve to weaken the structure.

The addition of flexible PVA chains into the intersheet gallery of stiff graphene oxide paper, in a manner that mimics the interaction between flexible proteins and stiff inorganic platelets in biocomposites, dramatically enhances the stiffness of the composite paper and decreases the role of water in the structure. In our experiment, stiffness increases continually as water content decreases up to a maximum value of 60 GPa (~50% increase over the case of pristine graphene oxide paper) when 7 wt % water is present. This behavior suggests that PVA can serve a similar role to that of water in graphene oxide paper, as subsequently confirmed by theoretical simulations, which reveal the presence of cooperative interactions between nonuniformly distributed small clusters of hydrogen-bonding groups located in the intersheet gallery. Such cooperativity enhances the stiffness of the nanocomposite in a similar fashion as that observed in natural biocomposites (e.g., spider silk and collagen).[12,13] Nevertheless, the large molecular structure of the PVA chains limits their interlayer dispersion, resulting in cavities and dangling, unutilized surface-bound functional groups on the surface of adjacent graphene oxide sheets. Fortuitously, the presence of small amounts of water molecules can fill in such underutilized interlayer connections, sufficiently saturating the hydroxyl and epoxy groups in the graphene oxide nanosheets. Together with optimizing the interactions between these groups (i.e., through their density and arrangement) and the intercalated PVA chains, tuning the water content in graphene oxide paper nanocomposites can clearly allow for the translation of the nanoscale hydrogen-bond network into macroscale mechanical properties. These findings can serve as guidance for future manipulation of the properties of other layered structures featuring hydrogen bonding networks.

EXPERIMENTAL SECTION

Materials. SP-1 graphite powder was used as received from Bay Carbon, Inc. (Bay City, MI). A narrow molecular weight (PDI = 1.2) sample of PVA (M_w = 2120 D) was obtained from Polymer Source, Inc. (Montreal, Québec, Canada). Ultrapure doubly deionized water (resistivity >18 MΩ cm) was obtained from an EMD Millipore (Billerica, MA) Milli-Q Biocel system.

Anodisc membranes (0.2 μm pore size, 47 mm diameter) from Whatman PLC (Maidstone, Kent, UK) were used during filtration for support of fabricated papers. Spectra/Por dialysis tubing (6–8 kD molecular weight cutoff (MWCO)) from Spectrum Laboratories, Inc. (Rancho Dominguez, CA) was utilized to remove excess ions from solution. Sonication was performed using a VC505 Vibra-cell probe sonicator (500 W) equipped with

a solid titanium–aluminum–vanadium tip (Sonics & Materials, Inc., Newton, CT). An Eppendorf model 5804 R centrifuge was employed for centrifugation.

Preparation of Graphene Oxide and Composite Dispersions. Graphite oxide (GO) was prepared using a modified Hummers procedure (see SI for synthetic details).[39–41] Aqueous graphene oxide dispersions were prepared following a reported literature procedure[42] by suspending GO in water and sonicating for 60 min (30% amplitude, 10 s pulses alternating with 10 s rest periods). Purification of this dispersion was achieved *via* a combination of centrifugation and dialysis (see SI for purification details). Composite dispersions of PVA and graphene oxide were prepared by combining an aqueous solution of PVA (30 mg in 20 mL of water) to a dilute aqueous graphene oxide dispersion (30 mL, 1 mg mL^{-1}).

Fabrication of Graphene Oxide and PVA-Graphene Oxide Nanocomposite Paper. Graphene oxide[8] and polymer composite papers[10] were prepared by filtering diluted graphene oxide dispersions or composite dispersions, respectively, through a Whatman Anodisc filter membrane. A Kontes Ultraware microfiltration apparatus with a fritted glass support base was utilized for vacuum filtration. After filtration, samples were air-dried until they could be peeled off the membrane for analysis.

Mechanical Analysis during Dehydration of Papers. Mechanical properties were evaluated using an RSA III (TA Instruments, New Castle, DE) dynamic mechanical analyzer (DMA). Samples for testing (2- to 6-mm wide and 20- to 40-mm long) were prepared from fabricated sheets of paper by compression-cutting with the sharp edge of a razor blade. Paper thickness was measured *via* scanning electron microscopy (SEM) images collected in the NEMS-MEMS Facility at Northwestern University using a field-emission gun Nova NanoSEM 600 microscope (FEI Co., Hillsboro, OR). These strips of graphene oxide and PVA-graphene oxide nanocomposite papers were loaded into the DMA oven at temperatures of 95 and 115 °C, respectively. Dynamic uniaxial tensile measurements (frequency = 1 Hz, strain = 0.025%) were carried out every 10 s under a flowing dry air stream for 12 h, until no further water could be removed from the sample. Identical strips of paper were loaded into the oven during annealing to allow for water content measurement without disturbing the dynamic evaluation.

Characterization. Water content was monitored using a C20X Compact Coulometric Karl Fischer titrator (Mettler-Toledo, Inc., Coloumbus, OH). Elemental analysis (EA) was performed at Atlantic Microlabs (Norcross, GA).

Molecular Models. In contrast to pristine (pure carbon) graphene, graphene oxide is heavily oxygenated, with hydroxyl (C–OH) and epoxide (C–O–C) functional groups heterogeneously distributed throughout the basal planes (see Figure 1).[5] As such, our molecular model was constructed from a basis of pristine graphene oxide sheets, with functional groups added to the graphene oxide plane in a random process according to the prescribed ratios of hydroxyls and epoxides. We constructed graphene oxide sheets with stoichiometries of $C_6O_2(OH)$ (e.g., two epoxy and one hydroxyl groups per six carbon atoms, distributed randomly on either side of the graphene basal plane). Two geometric arrangements were constructed for simulation (Figure 3a and 3b). The first model arrangement consisted of six layers of 25 Å × 25 Å graphene oxide sheets (Figure 3a). This model was implemented for computational efficiency to determine the equilibrated interlayer spacing as well as corresponding hydrogen-bond distributions. Such a stacked system is desirable to monitor average behavior throughout the multilayers. Periodic conditions were prescribed along each boundary, such that the relatively small system was representative of bulk graphene oxide paper.

The second model was a larger system, constructed specifically to be subject to loading in the transverse (shear) direction, similar to the experimental load conditions. The data obtained from the stacked first model were utilized to attain equilibrium configurations for this large model prior to application of strain. The final model consisted of four 50 Å × 100 Å GO sheets, which were alternatively offset by 10 Å along the *y*-axis (Figure 3b). Periodic conditions were prescribed along the *x* and *z* axes only, while loading was applied in the *y*-direction. Water molecules were added in the intersheet gallery between graphene oxide layers *via* a randomized distribution process. A short oligomer (five monomers in length) of PVA was minimized and equilibrated in an independent simulation with the same potential and software package described below. The equilibrated structure was then distributed within the interlayer planes in a randomized process (Figure 1b).

Simulation Methodology. The full atomistic investigations utilize the ReaxFF potential as implemented in the LAMMPS (Large-scale Atomic/Molecular Massively Parallel Simulator)[43] simulation package (http://lammps.sandia.gov/), previously developed for carbon–carbon interactions and hydrocarbon oxidation.[44,45] The first-principles-based ReaxFF force field has been shown to provide an accurate account of the chemical and mechanical behavior of hydrocarbons, graphite, diamond, carbon nanotubes, and other carbon nanostructures,[9,46–48] while it is capable of treating thousands of atoms with near quantum-chemical accuracy. The time step was chosen to be on the order of a fraction of femtoseconds (0.3×10^{-15} s) to ensure the stability of the simulations and reflect the relatively high vibrational frequency of the hydrogen atoms. All full atomistic simulations were subject to a microcanonical (*NVT*) ensemble, carried out at a temperature of 300 K. Temperature control was achieved using a Berendsen thermostat.[49] All MD simulations were performed using the massively parallelized modeling code LAMMPS, capable of running on large computing clusters. Energy minimization runs of the system are performed using a conjugate-gradient algorithm with an energy-convergence criterion implemented in the LAMMPS code. Details regarding the calculation of surface energy, determination of hydrogen bond presence, evaluation of interlayer spacing, and the analysis of theoretical stress–strain curves are available in the SI.

Acknowledgment. This work was supported by the NSF (Award No. DMR-0520513 through the MRSEC at Northwestern University, Award No. DMR-0819762 through the MRSEC at MIT, and Award No. CMMI-0928050 to L.C.B.) and ARO (Award No. W991NF-09-1-0541 to S.T.N. and M.J.B.). O.C.C. is an NSF-ACC fellow (Award No. CHE-0936924). We thank the Initiative for Sustainability and Energy (ISEN) at Northwestern for funding the purchase of some of the equipment used in this work. The atomistic calculations and the analysis were carried out using a parallelized LINUX cluster at MIT's Laboratory for Atomistic and Molecular Mechanics (LAMM). Visualization has been carried out using the VMD visualization package.[50] We thank Prof. Adri van Duin (Pennsylvania State University) for helpful discussions regarding the implementation of ReaxFF.

Supporting Information Available: Detailed experimental methods for the synthesis, exfoliation, and purification of graphene oxide, methodology for the determination of water content in graphene oxide paper samples, and details of theoretical methods. This material is available free of charge via the Internet at http://pubs.acs.org.

REFERENCES AND NOTES

1. Compton, O. C.; Nguyen, S. T. Graphene Oxide, Highly Reduced Graphene Oxide, and Graphene: Versatile Building Blocks for Carbon-Based Materials. *Small* **2010**, *6*, 711–723.
2. Wang, H.; Hao, Q.; Yang, X.; Lu, L.; Wang, X. Graphene Oxide Doped Polyaniline for Supercapacitors. *Electrochem. Commun.* **2009**, *11*, 1158–1161.
3. Sun, X.; Liu, Z.; Welsher, K.; Robinson, J.; Goodwin, A.; Zaric, S.; Dai, H. Nano-Graphene Oxide for Cellular Imaging and Drug Delivery. *Nano Res.* **2008**, *1*, 203–212.
4. Cai, W. W.; Piner, R. D.; Stadermann, F. J.; Park, S.; Shaibat, M. A.; Ishii, Y.; Yang, D. X.; Velamakanni, A.; An, S. J.; Stoller, M.; et al. Synthesis and Solid-State NMR Structural Characterization of ^{13}C-Labeled Graphite Oxide. *Science* **2008**, *321*, 1815–1817.
5. Lerf, A.; He, H.; Forster, M.; Klinowski, J. Structure of Graphite Oxide Revisited. *J. Phys. Chem. B* **1998**, *102*, 4477–4482.

6. Brunetaud, X.; Divet, L.; Damidot, D. Impact of Unrestrained Delayed Ettringite Formation-Induced Expansion on Concrete Mechanical Properties. *Cem. Concr. Res.* **2008**, *38*, 1343–1348.
7. Seah, K. H. W.; Hemanth, J.; Sharma, S. C. Tensile Strength and Hardness of Sub-Zero Chilled Cast Iron. *Mater. Des.* **1995**, *16*, 175–179.
8. Dikin, D. A.; Stankovich, S.; Zimney, E. J.; Piner, R. D.; Dommett, G. H. B.; Evmenenko, G.; Nguyen, S. T.; Ruoff, R. S. Preparation and Characterization of Graphene Oxide Paper. *Nature* **2007**, *448*, 457–460.
9. Medhekar, N. V.; Ramasubramaniam, A.; Ruoff, R. S.; Shenoy, V. B. Hydrogen Bond Networks in Graphene Oxide Composite Paper: Structure and Mechanical Properties. *ACS Nano* **2010**, *4*, 2300–2306.
10. Putz, K. W.; Compton, O. C.; Palmeri, M. J.; Nguyen, S. T.; Brinson, L. C. High-Nanofiller-Content Graphene Oxide-Polymer Nanocomposites *via* Vacuum-Assisted Self-Assembly. *Adv. Funct. Mater.* **2010**, *20*, 3322–3329.
11. Knowles, T.; Buehler, M. J. Nanomechanics of Functional and Pathological Amyloid Materials. *Nat. Nanotechnol.* **2011**, *6*, 469–479.
12. Keten, S.; Xu, Z.; Ihle, B.; Buehler, M. J. Nanoconfinement Controls Stiffness, Strength and Mechanical Toughness of β-Sheet Crystals in Silk. *Nat. Mater.* **2010**, *9*, 359–367.
13. Keten, S.; Buehler, M. J. Geometric Confinement Governs the Rupture Strength of H-Bond Assemblies at a Critical Length Scale. *Nano Lett.* **2008**, *8*, 743–748.
14. Sasaki, N.; Odajima, S. Stress-Strain Curve and Young's Modulus of a Collagen Molecule as Determined by the X-Ray Diffraction Technique. *J. Biomech.* **1996**, *29*, 655–658.
15. Gautieri, A.; Buehler, M. J.; Redaelli, A. Deformation Rate Controls Elasticity and Unfolding Pathway of Single Tropocollagen Molecules. *J. Mech. Behav. Biomed. Mater.* **2009**, *2*, 130–137.
16. Knauss, R.; Fleischer, G.; Gründer, W.; Kärger, J.; Werner, A. Pulsed Field Gradient NMR and Nuclear Magnetic Relaxation Studies of Water Mobility in Hydrated Collagen II. *Magn. Reson. Med.* **1996**, *36*, 241–248.
17. Boek, E. S.; Coveney, P. V.; Skipper, N. T. Molecular Modeling of Clay Hydration: A Study of Hysteresis Loops in the Swelling Curves of Sodium Montmorillonites. *Langmuir* **1995**, *11*, 4629–4631.
18. Hendricks, S. B.; Nelson, R. A.; Alexander, L. T. Hydration Mechanism of the Clay Mineral Montmorillonite Saturated with Various Cations. *J. Am. Chem. Soc.* **1940**, *62*, 1457–1464.
19. Buchsteiner, A.; Lerf, A.; Pieper, J. Water Dynamics in Graphite Oxide Investigated with Neutron Scattering. *J. Phys. Chem. B* **2006**, *110*, 22328–22338.
20. Lerf, A.; Buchsteiner, A.; Pieper, J.; Schöttl, S.; Dékány, I.; Szabó, T.; Boehm, H. P. Hydration Behavior and Dynamics of Water Molecules in Graphite Oxide. *J. Phys. Chem. Solids* **2006**, *67*, 1106–1110.
21. Putz, K. W.; Compton, O. C.; Segar, C.; An, Z.; Nguyen, S. T.; Brinson, L. C. Evolution of Order During Vacuum-Assisted Self-Assembly of Graphene Oxide Paper and Associated Polymer Nanocomposites. *ACS Nano* **2011**, *5*, 6601–6609.
22. Amorim, C. L. G.; Lopes, R. T.; Barroso, R. C.; Queiroz, J. C.; Alves, D. B.; Perez, C. A.; Schelin, H. R. Effect of Clay-Water Interactions on Clay Swelling by X-Ray Diffraction. *Nucl. Instrum. Methods Phys. Res., Sect. A* **2007**, *580*, 768–770.
23. Park, S.; An, J.; Suk, J. W.; Ruoff, R. S. Graphene-Based Actuators. *Small* **2010**, *6*, 210–212.
24. Scholz, W.; Boehm, H. P.; Untersuchungen Am Graphitoxid., VI. Betrachtungen Zur Struktur Des Graphitoxids. *Z. Anorg. Allg. Chem.* **1969**, *369*, 327–340.
25. Clauss, A.; Plass, R.; Boehm, H. P.; Hofmann, U. Untersuchungen Zur Struktur Des Graphitoxyds. *Z. Anorg. Allg. Chem.* **1957**, *291*, 205–220.
26. Fratzl, P.; Weinkamer, R. Nature's Hierarchical Materials. *Prog. Mater. Sci.* **2007**, *52*, 1263–1334.
27. Composite samples were heated at 115 °C (in contrast to the 95 °C heating temperature of pristine graphene oxide paper) to more efficiently evaporate water from the stucture.
28. Szabó, T.; Berkesi, O.; Forgó, P.; Josepovits, K.; Sanakis, Y.; Petridis, D.; Dékány, I. Evolution of Surface Functional Groups in a Series of Progressively Oxidized Graphite Oxides. *Chem. Mater.* **2006**, *18*, 2740–2749.
29. Paci, J. T.; Belytschko, T.; Schatz, G. C. Computational Studies of the Structure, Behavior Upon Heating, and Mechanical Properties of Graphite Oxide. *J. Phys. Chem. C* **2007**, *111*, 18099–18111.
30. Henry, D. J.; Yiapanis, G.; Evans, E.; Yarovsky, I. Adhesion between Graphite and Modified Polyester Surfaces: A Theoretical Study. *J. Phys. Chem. B* **2005**, *109*, 17224–17231.
31. Girifalco, L. A.; Lad, R. A. Energy of Cohesion, Compressibility, and the Potential Energy Functions of the Graphite System. *J. Chem. Phys.* **1956**, *25*, 693–697.
32. Cranford, S.; Sen, D.; Buehler, M. J. Meso-Origami: Folding Multilayer Graphene Sheets. *Appl. Phys. Lett.* **2009**, *95*, 123121.
33. Autumn, K.; Sitti, M.; Liang, Y. C. A.; Peattie, A. M.; Hansen, W. R.; Sponberg, S.; Kenny, T. W.; Fearing, R.; Israelachvili, J. N.; Full, R. J. Evidence for Van Der Waals Adhesion in Gecko Setae. *Proc. Natl. Acad. Sci. U.S.A.* **2002**, *99*, 12252–12256.
34. Due to the boundary conditions in the simulation, this value is most closely related to the Young's modulus, not the shear modulus. The sheets are subject to direct tension, and the stress measured is the uniaxial stress.
35. Jackson, A. P.; Vincent, J. F. V.; Turner, R. M. The Mechanical Design of Nacre. *Proc. R. Soc. London, Ser. B* **1988**, *234*, 415–440.
36. Penza, M.; Cassano, G. Relative Humidity Sensing by PVA-Coated Dual Resonator SAW Oscillator. *Sens. Actuators, B* **2000**, *68*, 300–306.
37. Keten, S.; Buehler, M. J. Asymptotic Strength Limit of Hydrogen-Bond Assemblies in Proteins at Vanishing Pulling Rates. *Phys. Rev. Lett.* **2008**, *100*, 198301/1–4.
38. Qin, Z.; Buehler, M. J. Cooperative Deformation of Hydrogen Bonds in Beta-Strands and Beta-Sheet Nanocrystals. *Phys. Rev. E* **2010**, *82*, 061906/1–9.
39. Hummers, W. S.; Offeman, R. E. Preparation of Graphitic Oxide. *J. Am. Chem. Soc.* **1958**, *80*, 1339–1339.
40. Kovtyukhova, N. I.; Ollivier, P. J.; Martin, B. R.; Mallouk, T. E.; Chizhik, S. A.; Buzaneva, E. V.; Gorchinskiy, A. D. Layer-by-Layer Assembly of Ultrathin Composite Films from Micron-Sized Graphite Oxide Sheets and Polycations. *Chem. Mater.* **1999**, *11*, 771–778.
41. Hirata, M.; Gotou, T.; Horiuchi, S.; Fujiwara, M.; Ohba, M. Thin-Film Particles of Graphite Oxide 1: High-Yield Synthesis and Flexibility of the Particles. *Carbon* **2004**, *42*, 2929–2937.
42. Stankovich, S.; Dikin, D. A.; Piner, R. D.; Kohlhaas, K. A.; Kleinhammes, A.; Jia, Y.; Wu, Y.; Nguyen, S. T.; Ruoff, R. S. Synthesis of Graphene-Based Nanosheets *via* Chemical Reduction of Exfoliated Graphite Oxide. *Carbon* **2007**, *45*, 1558–1565.
43. Plimpton, S. J. Fast Parallel Algorithms for Short-Range Molecular Dynamics. *J. Comput. Phys.* **1995**, *117*, 1–19.
44. Chenoweth, K.; van Duin, A. C. T.; Goddard, W. A. ReaxFF Reactive Force Field for Molecular Dynamics Simulations of Hydrocarbon Oxidation. *J. Phys. Chem. A* **2008**, *112*, 1040–1053.
45. Strachan, A.; Kober, E. M.; van Duin, A. C. T.; Oxgaard, J.; Goddard, W. A. Thermal Decomposition of RDX from Reactive Molecular Dynamics. *J. Chem. Phys.* **2005**, *122*, 054502.
46. van Duin, A. C. T.; Dasgupta, S.; Lorant, F.; Goddard, W. A.; ReaxFF, A Reactive Force Field for Hydrocarbons. *J. Phys. Chem. A* **2001**, *105*, 9396–9409.
47. Nielson, K. D.; van Duin, A. C. T.; Oxgaard, J.; Deng, W. Q.; Goddard, W. A. Development of the ReaxFF Reactive Force Field for Describing Transition Metal Catalyzed Reactions, with Application to the Initial Stages of the Catalytic

Formation of Carbon Nanotubes. *J. Phys. Chem. A* **2005**, *109*, 493–499.
48. Chen, N.; Lusk, M. T.; van Duin, A. C. T.; Goddard, W. A. Mechanical Properties of Connected Carbon Nanorings *via* Molecular Dynamics Simulation. *Phys. Rev. B* **2005**, *72*, 085416/1–9.
49. Berendsen, H. J. C.; Postma, J. P. M; Vangunsteren, W. F.; Dinola, A.; Haak, J. R. Molecular-Dynamics with Coupling to an External Bath. *J. Chem. Phys.* **1984**, *81*, 3684–3690.
50. Humphrey, W.; Dalke, A.; Schulten, K. VMD: Visual Molecular Dynamics. *J. Mol. Graphics* **1996**, *14*, 33–38.